arXiv:2108.04362v1 [astro-ph.SR] 9 Aug 2021

DO CORONAL LOOPS OSCILLATE IN ISOLATION?

Bradley W. Hindman
JILA, University of Colorado, Boulder, CO 80309-0440, USA and
Department of Applied Mathematics, University of Colorado, Boulder, CO 80309-0526, USA

Rekha Jain
School of Mathematics & Statistics, University of Sheffield, Sheffield S3 7RH, UK

ABSTRACT

Images of the solar corona by extreme-ultraviolet (EUV) telescopes reveal elegant arches of glowing plasma that trace the corona's magnetic field. Typically, these loops are preferentially illuminated segments of an arcade of vaulted field lines and such loops are often observed to sway in response to nearby solar flares. A flurry of observational and theoretical effort has been devoted to the exploitation of these oscillations with the grand hope that seismic techniques might be used as probes of the strength and structure of the corona's magnetic field. The commonly accepted viewpoint is that each visible loop oscillates as an independent entity and acts as a one-dimensional (1D) wave cavity for magnetohydrodynamic (MHD) kink waves. We argue that for many events, this generally accepted model for the wave cavity is fundamentally flawed. In particular, the 3D magnetic arcade in which the bright loop resides participates in the oscillation. Thus, the true wave cavity is larger than the individual loop and inherently multidimensional. We derive the skin depth of the near-field response for an oscillating loop and demonstrate that most loops are too close to other magnetic structures to oscillate in isolation. Further, we present a simple model of a loop embedded within an arcade and explore how the eigenmodes of the arcade and the eigenmodes of the loop become coupled. In particular, we discuss how distinguishing between these two types of modes can be difficult when the motions within the arcade are often invisible.

Subject headings: stars: magnetohydrodynamics (MHD) — Sun: corona — Sun: magnetic fields — Sun: oscillations — waves

1. INTRODUCTION

The bright coronal loops that manifest in EUV observations are often observed to vacillate in the aftermath of a solar flare (i.e., Aschwanden et al. 1999; Nakariakov et al. 1999; Wills-Davey & Thompson 1999). More recently it has been discovered that many loops constantly tremble at low-amplitude, even in the absence of large excitation events such as flares and coronal mass ejections (Nisticò et al. 2013; Anfinogentov et al. 2013; Wang et al. 2012; Duckenfield et al. 2018). The suggestion that the observed loop oscillations are resonant magnetohydrodynamic (MHD) waves and that the frequencies of these resonant modes might be used as a seismic probe of the corona (Roberts et al. 1984) has spurred the development of the entire discipline of coronal seismology—see the review by Nakariakov & Kolotkov (2020).

The seminal works of Edwin & Roberts (1983) and Roberts et al. (1984) have become the cornerstone of coronal seismology. These studies theoretically examine wave propagation in coronal loops and highlight the important connection of these waves to coronal observations. The models introduced in these papers popularized the approximation of a coronal loop as a slender, straight, magnetic tube and, in so doing, have become the theoretical backbone of seismic analysis of the properties of coronal loops. Under such a thin-tube assumption, there are two forms of wave that predominate: the kink

(transverse) and sausage (longitudinal) oscillations. It is believed that the observed vacillation of coronal loops is due to standing kink waves trapped in an essentially 1D cavity lying between the two foot points of the loop in the photosphere (i.e., Aschwanden et al. 1999; Nakariakov et al. 1999; Goddard et al. 2016)

The model of Edwin & Roberts (1983) demonstrates that when the magnetic flux tube is thin, the kink wave propates along the loop at a well-defined phase speed, c_k, called the kink speed,

$$c_k^2 = \frac{B_0^2 + B_e^2}{4\pi (\rho_0 + \rho_e)} \ . \tag{1}$$

In this expression, ρ_0 and ρ_e are, respectively, the mass densities inside the loop and in the coronal environment surrounding the loop. Similarly, B_0 and B_e are the magnetic field strength inside and outside the loop. Since undulating coronal loops are thought to be overdense with $\rho_0 \gg \rho_e$ (Lenz et al. 1999; Winebarger et al. 2003; Reale 2014) and $B_0 \approx B_e$, the Alfvén speed in the loop is less than the Alfvén speed in the surrounding corona, and the kink speed is intermediate, with a value between the two Alfvén speeds. The goal of coronal seismology is to measure the frequency ω and wavenumber k_z of the oscillation and thus deduce the kink speed, $c_k = \omega/k_z$, which provides a weighted average of the magnetic field strength.

hindman@solarz.colorado.edu

The model of Edwin & Roberts (1983) makes four fundamental assumptions:

- The curvature of the coronal loop's axis can be ignored.

- The loop and the surrounding corona are invariant along the loop.

- The coronal loop lacks substructure in radius and azimuth that modify the kink wave frequency.

- The corona surrounding the loop lacks structure that causes reflections.

The implications of the first three of these assumptions have been studied extensively. The frequency shifts and polarization caused by loop curvature have been explored and characterized (e.g., Terradas et al. 2006; Gruszecki et al. 2007; Ruderman 2009; Van Doorsselaere et al. 2009; Pascoe & De Moortel 2014; Hindman & Jain 2015; Thackray & Jain 2017). Frequency shifts to the various longitudinal overtones have been exploited as a means to assess variation in the properties of the loop along its length (Andries et al. 2005; Goossens et al. 2006; Dymova & Ruderman 2006; Díaz et al. 2007; McEwan et al. 2008; Ruderman et al. 2008; Verth & Erdélyi 2008; Orza et al. 2012; Jain & Hindman 2012). Theoretical work has shown that closely packed magnetic threads oscillate as a collective entity and the resulting kink speed is an average of the properties of all of the threads (e.g., Terradas et al. 2008). Conversely, the importance and applicability of the fourth assumption have not received sufficient attention. Observations suggest that the oscillation of a loop is often coupled to the oscillation of nearby magnetic structures (Schrijver & Brown 2000; Schrijver et al. 2002; Verwichte et al. 2004, 2009; Jain et al. 2015; Li et al. 2017). The animation appearing as Figure 1 illustrates the problem. This sequence of images was obtained by the Atmospheric Imaging Assembly (AIA) on board the *Solar Dynamics Observatory* (SDO) using the Fe IX 171 Å bandpass. After a flare, MHD waves can be seen to propagate back and forth across the entire active region. Since, the waves propagate across field lines they must be fast magnetic-pressure waves instead of pure kink waves. Further, the coronal loops are not the only features that sways back and forth. There are correlated motions of the loops, of the arcade of field lines in which the loops are embedded, and in fact of the entire active region. From movies like Figure 1 it is clear that coronal loops rarely oscillate in isolation.

Here, we will coarsely examine some of the issues associated with structuring of the environment around the loop. In particular we hope to address the question, "Under what conditions can a coronal loop oscillate in isolation, such that the standard model of loop oscillations can be applied?" In order to assess these issues, we need to consider two possibilities that can occur simultaneously for waves of different frequency: evanescence or propagation within the coronal environment and the host arcade. We will examine these two possibilities separately in sections 2 and 3. In section 4, we will present our conclusions and discuss the implications of those conclusions on the reliability of coronal seismology.

2. EVANESCENT WAVES IN THE EXTERNAL FLUID: SKIN DEPTH

In order for kink waves to be a resonant oscillation of a coronal loop, the MHD wave's energy density must be strongly concentrated within the loop or in the immediate environs of the loop. Usually, this is accomplished by the wave being evanescent outside the loop. But even if evanescent, the wavefield penetrates some distance into the fluid surrounding the loop in a region called the near field. The exponential decay length of this penetration, or the *skin depth*, can be derived without a detailed consideration of the loop's geometry and cross section. The result depends on the Alfvén speed of the external media and the temporal frequency of the wave. We will perform this calculation here and then focus on thin flux tubes with a circular cross section.

2.1. *Derivation of the Skin Depth*

We assume that the Sun's corona is magnetically dominated and ignore buoyancy and gas pressure. If the fluid exterior to the loop is uniformly magnetized and possesses a spatially constant density, the MHD equations for the fluid velocity and magnetic pressure fluctuation become particularly simple. The magnetic pressure fluctuation, Π, obeys a standard wave equation (e.g., Díaz et al. 2003; Roberts 2019),

$$\frac{\partial^2 \Pi}{\partial t^2} = V_e^2 \, \nabla^2 \Pi \, , \qquad (2)$$

and the fluid velocity $\boldsymbol{u}$ simultaneously obeys

$$\frac{\partial^2 \boldsymbol{u}}{\partial t^2} - V_e^2 \frac{\partial^2 \boldsymbol{u}}{\partial z^2} = -\frac{1}{\rho_e} \boldsymbol{\nabla}_\perp \frac{\partial \Pi}{\partial t} \, , \qquad (3)$$

where V_e and ρ_e are the Alfvén speed and mass density of the external fluid, respectively. The spatial coordinate z is aligned with the magnetic field and the differential operator $\boldsymbol{\nabla}_\perp$ is the gradient in the plane perpendicular to the magnetic field. These equations describe only Alfvén waves and fast MHD waves. The slow magnetoacoustic waves are missing, because, as already stated, we have adopted a "cold-plasma" limit where the gas pressure is ignored. Alfvén waves arise from the condition $\Pi = 0$ and fast waves occur when the magnetic pressure is nonzero.

From Equation (2), we can directly extract an expression for the evanescence length lateral to the field lines. By assuming exponential solutions of the form,

$$\Pi = e^{-i\omega t} \, e^{ik_z z} \, \tilde{\Pi}\left(\boldsymbol{x}_\perp\right) \, , \qquad (4)$$

we obtain an equation for the transverse variation of the magnetic pressure,

$$\nabla_\perp^2 \Pi = \left(k_z^2 - \frac{\omega^2}{V_e^2} \right) \, . \qquad (5)$$

In these last two equations, ω is the temporal frequency, k_z is the longitudinal wavenumber, and $\boldsymbol{x}_\perp$ is the component of the position vector that is transverse to the magnetic field.

Up to this point in our derivation, we have implicitly assumed that the curvature of the magnetic field lines can be ignored, but we have not assumed anything about the shape or geometry of the loop's cross-section. From

Equation (5) it is clear that the specific shape of the cross-section does not play much of a role since the Laplacian operator is isotropic. For example, if we assume that the fast waves are evanescent in the external fluid, and adopt an exponential form that is valid in Cartesian geometry,

$$\Pi = e^{-i\omega t}\, e^{ik_z z}\, \exp\left(-\boldsymbol{\alpha} \cdot \boldsymbol{x}_\perp\right) \;, \qquad (6)$$

we obtain the following dispersion relation

$$\omega^2 = \left(k_z^2 - \alpha^2\right) V_e^2 \;. \qquad (7)$$

The skin depth Δ is the reciprocal of the decay rate, $\Delta = 1/\alpha$. Hence, the skin depth depends on the frequency, longitudinal wavenumber, and the Alfvén speed,

$$\frac{1}{\Delta^2} = k_z^2 - \frac{\omega^2}{V_e^2} \;. \qquad (8)$$

The same skin depth is achieved if we assume cylindrical symmetry (e.g., Edwin & Roberts 1983),

$$\Pi = e^{-i\omega t}\, e^{ik_z z}\, e^{i\mu\phi}\, K_\mu\left(\alpha r\right) \;, \qquad (9)$$

where ϕ is the azimuth, r is the cylindrical radius, μ is the azimuthal order, and K_μ is a modified Bessel function of the second kind. This cylindrical form produces the same dispersion relation and skin depth. The skin depth is independent of the transverse geometry.

From Equation (8), we can extract a lower limit for the skin depth. Clearly, the skin depth will be smallest (and the transverse decay rate the largest) when the frequency is low (i.e., $\omega \ll k_z V_e$) and the second term on the right-hand side can be ignored,

$$\Delta > k_z^{-1} \;. \qquad (10)$$

We re-emphasize, that this lower limit is independent of the shape of the loop's cross section and on the Alfvén speed. Further, its independent of direction. For example, if one considers a loop with a rectangular cross-section, the external wave solutions can have different decay lengths in the two transverse directions (e.g., Díaz et al. 2003; Arregui et al. 2007). But, increased lateral confinement in one direction leads to decreased lateral confinement in the other because the decay rates in the two directions add in quadrature,

$$\frac{1}{\Delta^2} = \alpha^2 = \alpha_x^2 + \alpha_y^2 = \frac{1}{\Delta_x^2} + \frac{1}{\Delta_y^2} \;. \qquad (11)$$

In the previous expression, α_x and α_y are the two transverse components of vector $\boldsymbol{\alpha}$.

We can find a more nuanced expression for the skin depth if we assume that the loop is thin and has a circular cross section. With these two assumptions we can replace the frequency with the well-known dispersion relation for kink waves on a slender magnetic flux tube, $\omega = k_z c_k$, where c_k is given by Equation (1) (e.g., Edwin & Roberts 1983). Continuity of the total pressure under the cold-plasma approximation dictates that the magnetic field has the same strength inside and outside the loop, $B_0 = B_e$. Hence, the kink speed can be expressed in terms of the external Alfvén speed and the overdensity ratio of the loop, $f \equiv \rho_0/\rho_e$,

$$c_k^2 = \frac{B_e^2}{2\pi\left(\rho_0 + \rho_e\right)} = \frac{2V_e^2}{f + 1} \;. \qquad (12)$$

Substituting this kink speed into the expression for the skin depth, Equation (8), produces a frequency-independent result,

$$\Delta = \left(\frac{f+1}{f-1}\right)^{1/2} k_z^{-1} \;. \qquad (13)$$

The leading coefficient involving the square root is always greater than one; hence, the same lower limit that we derived earlier applies, $\Delta > 1/k_z$. Here, we now see that this lower limit is approached as the loop becomes extremely dense compared to the surrounding fluid, $\rho_0 \gg \rho_e$ or $f \gg 1$. In practice, the high overdensity limit is usually valid. Typical "warm" coronal loops (temperatures less than 3 MK) often have an overdensity ratio of 1000 or more (e.g., Winebarger et al. 2003).

Finally, if we assume that the kink wave is a standing-wave resonance arising from reflections at the two foot points where the magnetic loop intersects the photosphere, we can relate the longitudinal wavenumber k_z, and subsequently the skin depth Δ, to the length of the loop L,

$$k_z = \frac{m\pi}{L} \;, \qquad \Delta = \left(\frac{f+1}{f-1}\right)^{1/2} \frac{L}{m\pi} \;. \qquad (14)$$

In these expressions, m is the longitudinal mode order, with $m = 1$ corresponding to the fundamental mode which lacks nodes in the velocity eigenfunction. Almost all observed coronal loop oscillations are thought to be oscillating in the fundamental mode and hence we will focus our attention on $m = 1$.

Since the lower limit for the skin depth of the fundamental mode, $\Delta > L/\pi$, depends only on the loop length (and not the Alfvén speed or wave frequency), the limit is useful and easily applied. Unfortunately, it is also rather stringent because the skin depth is so large. For example, for a coronal loop whose axis is semicircular, the skin depth equals the radius of curvature and, accordingly, the loop's maximum height above the photosphere. The skin depth is also comparable to the spatial extent of many coronal arcades. Consider a "typical" coronal loop with a length of 100 Mm and an overdensity ratio of 10; the skin depth would be 35 Mm. Loops with a more moderate overdensity can have a significantly longer skin depth. For instance, a 100 Mm loop that is twice as dense as its surroundings ($f = 2$) would have a skin depth that is nearly 50% longer, $\Delta = 55$ Mm.

2.2. Is a Coronal Loop Isolated?

If the coronal loop is to oscillate in isolation, there cannot be any nearby magnetic or density structures that efficiently scatter or reflect MHD waves, such as another coronal loop. Any such structure that is sufficiently close will couple to the coronal loop through wave scattering in their overlapping near fields. A good rule of thumb is that the loop will interact appreciably with any scattering structure that is within one or two skin depths. For example, Luna et al. (2008) and Van Doorsselaere

et al. (2008) found that this coupling could shift the frequency of kink oscillations up or down by 25% or more if two identical tubes were close—see Figure 3 of Luna et al. (2008) and Figure 6 of Van Doorsselaere et al. (2008). Both of these studies characterized the "closeness" of the tubes in terms of the ratio d/a, where d is the separation between the centers of the two tubes and a is the radius of the tubes. A more direct criterion is based on whether the two tubes suffer near-field coupling, which depends solely on the ratio of the separation to the skin depth, d/Δ. It is straightforward to work out the skin depth for these studies by using Equation (14). In Figure 3 of Luna et al. (2008) and Figure 6 of Van Doorsselaere et al. (2008), the skin depth is 3.5 times the tube radius a. Thus, in both of these studies, it is clear that strong coupling occurs when $d/\Delta < 1$ and modest coupling persists for separations of up to two skin depths.

For many coronal loops, satisfying the criteria that no other magnetic structure lies within a skin depth is exceedingly difficult. In the catalog of loop oscillations published by Nechaeva et al. (2019), 12 of the 20 loops have lengths exceeding 300 Mm. Such loops will have skin depths in excess of 100 Mm. It is difficult to believe that the corona lacks scattering structures over such distances when active regions themselves are ordered on a similar scale. There have been a variety of events where coupling between nearby loops has been directly observed (e.g., Schrijver & Brown 2000; Schrijver et al. 2002; Verwichte et al. 2004; Jain et al. 2015). In Jain et al. (2015) two loops with similar length (~ 160 Mm) were seen to oscillate in concert. Figure 2 shows an image of the two loops taken in the 171 Å bandpass of the Atmospheric Imaging Assembly (AIA; Lemen et al. (2012)) aboard the *Solar Dynamics Observatory* (*SDO*). Jain et al. (2015) attributed the similarity in phase and initiation time of the two loops to the near cotemporal excitation by a common driving event. However, considering that the loops were only separated by 3.5 Mm (see Figure 2), these loops were deep within each other's near-field regions. Loops of the measured length, 160 Mm, will have a skin depth exceeding 50 Mm. Since the loop separation is only 7% of the skin depth, it should be no surprise that the two loops were coupled and oscillated in synchronicity. This would be true even if the excitation event (probably a wavefront launched by a nearby flare) only acted to generate waves on one of the loops. Oscillation of one loop would cause sympathetic vibration of the neighboring loop. In fact, far more than just the two loops under consideration were coupled. The skin depth of 50 Mm corresponds to roughly 70 arcsec. Most of the field of view in Figure 2 is within a single skin depth of the two loops that were studied. Hence, to truly understand the oscillations excited by the nearby flare, one needs to examine the entire active region, as all of the magnetic features are coupled to some degree. This coupling of many magnetic structures may also explain the slight phase shift that was observed between the two loops by Jain et al. (2015). When only two loops are coupled, the collective modes involve either in-phase or antiphase motions of the two tubes (e.g., Luna et al. 2008, 2009; Van Doorsselaere et al. 2009). But, such clear phase correlations are not expected when three or more oscillating structures are coupled.

Even if a loop is isolated from other magnetic structures it's not free from the tyranny of the skin depth. Most calculations and seismic analyses of the oscillation frequencies assume that the curvature of the loop's axis can be ignored. However, for a loop of length L whose axis is semicircular, the radius of curvature of the loop is identical to the skin depth, L/π. Thus, the loop should undergo significant "self-interaction" as the foot points of the loop lie within a skin depth of each other. Of course, most loops will not form perfect semicircles. Often, coronal loops are taller and with closer foot points than a semicircular loop with identical length. For such "tall" loops, the foot points are closer than a skin depth and the self-interaction will be even stronger. Even low-lying loops with farspread foot points are not immune. All portions of such a loop will lie within a skin depth of the photosphere itself and we should expect significant scattering from the photospheric surface that is not accounted for by the simple line-tying boundary conditions imposed at the foot points.

3. PROPAGATING FAST WAVES: REFLECTIONS FROM EXTERNAL STRUCTURES

The coronal environment surrounding a coronal loop is usually an arabesque of magnetic structures. Coronal loops are arranged in magnetic arcades like the warp of a loom and these arcades are just one piece of a larger magnetic active region. In the immediate aftermath of a nearby flare, waves are everywhere within the active region. Fast MHD waves can be seen racing across field lines and often waves can be observed to bounce back and forth across an arcade or the active region. The animation shown as Figure 1 typifies such wave motion. Propagating waves are seen to be ubiquitous and omnipresent.

Such behavior should be expected. The flare that excites oscillations on the coronal loop is rarely if ever located on any of the field lines that pass through the loop. Hence, fast MHD waves must travel from the flaring site, across field lines, to the coronal loop where it excites kink waves. There is no reason to suppose that the fast wave that performs this excitation does not excite oscillations on other magnetic structures as it passes. These excited waves should bounce around the active region until scattered, radiated, or dissipated.

The back and forth motion of the field lines within arcades suggests that the arcade or active region may have resonances of its own, in addition to those of coronal loops. Such arcade oscillations can clearly be seen to have significant amplitude in coronal imagery (see Figure 1). Hence, any potential arcade resonances should have large enough amplitude to provoke substantial coupling with the loop oscillations. Whether they do so or not will depends on whether the arcade resonances have frequencies that are similar to the loop resonances. Here we explore the possibility of coupling between the loop resonances and arcade resonances using a simple model that is designed to be illustrative instead of predictive.

3.1. *Simple Model of an Arcade and Loop System*

We will model the arcade as a thin, curved, magnetic sheet with a thickness of D and with field lines that pierce the photosphere twice. One can think of the arcade as the roof of a Quonset hut and the photosphere

as the ground. The two ribbons that demark the intersection of the sheet with the photosphere are parallel to each other and parallel to the arcade's geometrical axis, $\hat{\boldsymbol{x}}$ (see Figure 3). The arcade's magnetic field $\boldsymbol{B}$ lacks shear such that the field is everywhere perpendicular to arcade's axis, $\boldsymbol{B} \cdot \hat{\boldsymbol{x}} = 0$. Therefore, for a suitably thin sheet, we may assume that the length of each field line in the corona—from photosphere to photosphere—is a constant value L. In the axial direction, the magnetic sheet spans a finite width of $2W$ and the coronal loop (shown in red in Figure 3) occupies the center of the arcade with an axial extent of 2δ. The loop therefore has a rectangular cross section with dimensions $2\delta \times D$ and a longitudinal length of L.

To keep the mathematics simple, we will make the standard assumption of ignoring the curvature of the field lines in the MHD equations. This straightening of the geometry permits us to utilize a coordinate system $\boldsymbol{x} = (x, y, z)$ that is coincident with the local Frenet coordinates for the field lines. The tangential coordinate z measures the distance along each field line, with $z = 0$ and $z = L$ corresponding to the two points where the field line pierces the photosphere. The coordinate x, points in the direction of the field line's binormal and measures distances along the axis of the arcade. We place the origin, $x = 0$, in the middle of the loop and arcade system; hence, the arcade spans the domain $x \in [-W, W]$ and the loop spans $x \in [-\delta, \delta]$. The third coordinate, y, is antiparallel to the direction of the principle curvature of the field line, and points normal to the magnetic sheet that forms the arcade. The geometry of the loop-arcade system is a magnetized slab (loop) embedded within a less dense magnetized slab (arcade)—see Figure 3.

As in the derivation of the skin depth, we will assume that the corona is magnetically dominated and hence ignore gravity and gas pressure. Therefore, to enforce stability in this straightened geometry, we must assume that the magnetic pressure is uniform. This is most easily accomplished by adopting a constant magnetic field $\boldsymbol{B} = B_0 \hat{\boldsymbol{z}}$. To ensure that waves can be trapped in the coronal loop, we will consider a piece-wise constant mass density and Alfvén speed, where the density in the arcade is ρ_e and the density in the loop is ρ_0. The corresponding Alfvén speeds are V_e and V_0. We assume that the loop is overdense compared to the surrounding arcade $\rho_0 > \rho_e$ and, correspondingly, the Alfvén speed is reduced in the loop, $V_0 < V_e$.

3.1.1. *Plane-Wave Solutions*

Since, we have adopted a low-β approximation and the Alfvén speed is uniform within the loop and separately within the arcade, the waves are described by Equations (2) and (3) with the appropriate Alfvén speed and density for each region. Since, we have ignored gas pressure and buoyancy, the motions are purely transverse (i.e., $\boldsymbol{u} = u_x \hat{\boldsymbol{x}} + u_y \hat{\boldsymbol{y}}$). The solutions to Equations (2) and (3) are plane waves with frequency ω and wavenumber $\boldsymbol{k} = k_x \hat{\boldsymbol{x}} + k_y \hat{\boldsymbol{y}} + k_z \hat{\boldsymbol{z}}$,

$$\Pi \sim \exp(-i\omega t) \exp(i\boldsymbol{k} \cdot \boldsymbol{x}) \,, \qquad (15)$$

$$\boldsymbol{u} = \frac{\omega \boldsymbol{k}_\perp}{\rho \Omega^2} \Pi \,, \qquad (16)$$

where we have defined $\Omega^2 \equiv \omega^2 - k_z^2 V^2$ and the frequency and wavenumber are related through a local dispersion relation

$$\omega^2 = \left(k_x^2 + k_y^2 + k_z^2 \right) V^2 \,. \qquad (17)$$

In these expressions the Alfvén speed, V takes on the value of either V_0 or V_e depending on whether we are considering the region inside or outside the loop. The wavenumber $\boldsymbol{k}_\perp$ is the component of the wavenumber $\boldsymbol{k}$ that is transverse to the magnetic field, i.e., $\boldsymbol{k}_\perp = k_x \hat{\boldsymbol{x}} + k_y \hat{\boldsymbol{y}}$. For those waves that are laterally evanescent, the transverse wavenumber is related to the lateral decay rate, $\boldsymbol{k}_\perp = i\boldsymbol{\alpha}$.

3.1.2. *Boundary and Interface Conditions*

We apply boundary conditions, two in each spatial dimension, that are chosen largely for convenience and to develop a simple, easily understood example. For the boundary conditions in the longitudinal coordinate z, we recognize that the photosphere can be treated as an extremely dense immovable plasma. Hence, we adopt the standard line-tying condition that the velocity must vanish at the two foot points of the field line, i.e., $\boldsymbol{u} = 0$ at $z = 0$ and $z = L$. This requirement quantizes the tangential wavenumber, mandating that $k_z = m\pi/L$, with m being a positive integer. The longitudinal wavenumber will be the same in both regions, inside and outside the loop.

In the direction normal to the arcade's sheet, y, we adopt impenetrable boundaries at the top and bottom surfaces of the sheet, $y = \pm D/2$, and require that the fluid motion is unvarying across the sheet, $k_y = 0$. We fully recognize that the boundary condition of impenetrability is a rather poor one; but without it, motions in the two transverse directions become inherently coupled and a tremendous degree of complexity ensues (see for example Joarder & Roberts 1992). By imposing impenetrable boundaries and spatial invariance in the y direction, we ensure that motions are allowed only in the axial direction x and correspond to so called 'horizontal' oscillations of the loop.

For the third set of boundary conditions, we adopt "open boundaries" at the ends of the arcade in the axial direction, i.e., we require that magnetic pressure fluctuation vanish at $x = \pm W$. A quick examination of the PDEs, Equations (2) and (3), reveals that this condition is equivalent to requiring that the axial derivative of the axial velocity vanishes at both end points, $\partial u_x / \partial x = 0$. Other homogeneous boundary conditions in the axial direction could be implemented. For example, we could enforce impenetrable boundaries $u_x = 0$, or we could match to an extremely diffuse coronal background and require evanescent solutions that decay away from the arcade. However, doing so does not fundamentally change the structure of the eigenfunctions or the eigenfrequencies, but can involve a large degree of added complexity.

With these choices of boundary conditions, the magnetic pressure and the velocity must have the following functional form,

$$\Pi = \sin\left(\frac{m\pi}{L} z\right) e^{-i\omega t}$$

$$
\times \begin{cases} A_1 \cos{(k_x x)} + A_2 \sin{(k_x x)} & \text{for } |x| < \delta \\ A_3 \sin{[k_x (W - x)]} & \text{for } |x| > \delta \end{cases} \quad (18)
$$

$$
u_x = \frac{i\omega k_x}{\rho \Omega^2} \sin\left(\frac{m\pi}{L}z\right) e^{-i\omega t}
$$

$$
\times \begin{cases} A_1 \sin{(k_x x)} - A_2 \cos{(k_x x)} & \text{for } |x| < \delta \\ A_3 \cos{[k_x (W - x)]} & \text{for } |x| > \delta \end{cases} \quad (19)
$$

with A_1, A_2, and A_3 being real-valued amplitudes.

The final requirements that are needed to fully specify the solution are matching conditions that apply at the interfaces between the loop and arcade, $x = \pm\delta$. We require that both the magnetic pressure and the axial velocity are continuous across these interfaces. The simultaneous solution of these four interface constraints has a solvability condition that results in a global, transcendental dispersion relation. The modes that are odd functions about the center of the loop, $x = 0$, have a different dispersion relation than those that are even. The solutions that have an even velocity eigenfunction (or odd magnetic pressure fluctuation) are called kink waves and those that have an odd velocity function (or even magnetic pressure fluctuation) are called sausage waves (Edwin & Roberts 1982). It is a confusing matter of nomenclature, that both these slab modes, kink and sausage, are fast MHD waves (remember we have no slow waves because $\beta = 0$). In cylindrical geometry, for a flux tube with low but finite β, the kink wave is also a type of fast wave but the sausage wave is a varicose slow MHD wave.

The dispersion relations of the two waves modes are as follows,

$$
\text{kink}: \ k_e \tan{[k_e(W - \delta)]} + k_0 \tan{(k_0 \delta)} = 0 \ , \quad (20)
$$
$$
\text{sausage}: \ k_e \tan{[k_e(W - \delta)]} - k_0 \cot{(k_0 \delta)} = 0 \ , \quad (21)
$$

where k_e and k_0 are the axial wavenumbers in the arcade and in the loop, respectively,

$$
k_e^2 = \frac{\omega^2}{V_e^2} - \left(\frac{m\pi}{L}\right)^2 = \frac{\Omega_e^2}{V_e^2} \ , \quad (22)
$$

$$
k_0^2 = \frac{\omega^2}{V_0^2} - \left(\frac{m\pi}{L}\right)^2 = \frac{\Omega_0^2}{V_0^2} \ . \quad (23)
$$

Note, each region has a distinct cutoff frequency, $\omega_c = m\pi L/V$, which depends on the loop length L and the appropriate Alfvén speed for the region under consideration, $V = V_e$ or $V = V_0$. For frequencies above the cutoff, the waves are axially propagating, $k_e^2 > 0$ or $k_0^2 > 0$.

3.1.3. *Eigenfrequencies and Eigenfunctions*

The dispersion relations can be solved numerically for the wave frequency as a function of the two Alfvén speeds, V_0 and V_e, the loop length L, the half-width of the loop δ, the breadth of the arcade $2W$, and the longitudinal mode order m. In order to reduce the number of free parameters that the frequency depends on, we consider only the longitudinal fundamental $m = 1$, and we use the loop length L and the Alfvén crossing time L/V_0 to nondimensionalize. With this change of variable, the dispersion relation can be solved for the nondimensional frequency, $\varpi \equiv (L/V_0)\omega$, in terms of three ratios: the

nondimensional half width of the loop δ/L, the nondimensional breadth of the arcade $2W/L$, and the overdensity ratio $f = \rho_0/\rho_e = V_e^2/V_0^2$.

Once an eigenfrequency has been obtained through the transcendental dispersion relation, the magnetic pressure and velocity eigenfunctions that are associated with that frequency are given by the following equations,

Kink Modes

$$
\Pi = \frac{B_0^2}{4\pi} \sin\left(\frac{m\pi}{L}z\right) e^{-i\omega t} \quad (24)
$$

$$
\times \begin{cases} \sin(k_0 x) & \text{for } |x| < \delta \\ \dfrac{\text{sgn}(x) \sin{(k_0 \delta)}}{\sin{[k_e(W - \delta)]}} \sin{[k_e(W - |x|)]} & \text{for } |x| > \delta \end{cases}
$$

$$
u_x = i\frac{\omega}{k_0} \sin\left(\frac{m\pi}{L}z\right) e^{-i\omega t} \quad (25)
$$

$$
\times \begin{cases} -\cos(k_0 x) & \text{for } |x| < \delta \\ \dfrac{k_0 \sin{(k_0 \delta)}}{k_e \sin{[k_e(W - \delta)]}} \cos{[k_e(W - |x|)]} & \text{for } |x| > \delta \end{cases}
$$

Sausage Modes

$$
\Pi = \frac{B_0^2}{4\pi} \sin\left(\frac{m\pi}{L}z\right) e^{-i\omega t} \quad (26)
$$

$$
\times \begin{cases} \cos(k_0 x) & \text{for } |x| < \delta \\ \dfrac{\cos{(k_0 \delta)}}{\sin{[k_e(W - \delta)]}} \sin{[k_e(W - |x|)]} & \text{for } |x| > \delta \end{cases}
$$

$$
u_x = i\frac{\omega}{k_0} \sin\left(\frac{m\pi}{L}z\right) e^{-i\omega t} \quad (27)
$$

$$
\times \begin{cases} \sin(k_0 x) & \text{if } |x| < \delta \\ \dfrac{\text{sgn}(x)k_0 \cos{(k_0 \delta)}}{k_e \sin{[k_e(W - \delta)]}} \cos{[k_e(W - |x|)]} & \text{if } |x| > \delta \end{cases}
$$

For any set of parameter values, there are of course a countable infinity of eigenfrequencies. Figure 4 is a mode diagram that illustrates the mode frequencies as a function of the loop's half-width for an overdensity ratio of $f = 10$ and an arcade breadth of $2W/L = 3$. Only the longitudinal fundamental, $m = 1$, is illustrated. The blue curves indicate the frequency of kink modes and the red curves show sausage modes. We label each member of the sequence by the axial mode order n. This order is a non-negative integer that indicates the number of nodes that appear in the axial direction for the velocity eigenfunction, u_x. The gravest mode, $n = 0$, corresponds to the traditional kink oscillation of a thin coronal loop. It lacks nodes in the velocity eigenfunction, has a single pressure node in the middle of the loop, and is evanescent in the region outside the loop. In Figure 4, the two horizontal black lines indicate cutoff frequencies in the loop (dash-dotted line), $m\pi V_0/L$, and in the arcade (dotted line), $m\pi V_e/L$. Waves with frequencies less than the respective cutoff are axially evanescent ($k_x^2 < 0$) in the associated region.

The higher orders $n > 0$, correspond to kink and sausage modes with additional axial nodes, i.e., axial overtones. For thin loops (small δ) all of the overtones

propagate axially in the arcade, $k_e^2 > 0$. Only for sufficiently fat loops does the frequency of an overtone drop below the cutoff frequency for the arcade and become evanescent outside the loop. The threshold loop thickness varies from overtone to overtone.

A prominent feature of the dispersion curves for all of the overtones are a sequence of avoided crossings. These crossings occur when a node in the velocity eigenfunction passes across the loop-arcade boundary and can be thought of as those parameter values where a resonance of the loop and a resonance of the arcade have similar frequencies. If the arcade were to be very wide with extremely low density (high Alfvén speed), the modes of the loop would be given by a transcendental dispersion relation (Edwin & Roberts 1982),

$$\text{kink}: \quad -|k_e| + k_0 \tan(k_0 \delta) = 0 \,, \quad (28)$$
$$\text{sausage}: \quad -|k_e| - k_0 \cot(k_0 \delta) = 0 \,. \quad (29)$$

These equations can be derived from Equations (20) and (21), by assuming that $f \gg 1$ and $W \gg \delta$. The resulting sausage waves and kink waves are shown as dotted red and blue curves in Figure 4. In the same limit of a very dense loop ($f \gg 1$), the modes of the arcade correspond to those waves that treat the loop as immovable, i.e., those that have $u_x = 0$ at the loop-arcade boundaries, $x = \pm \delta$. One can easily derive from Equations (25) and (26) the value of the axial wavenumber which generates a node at this interface,

$$k_e = \frac{(j + 1/2)\,\pi}{W - \delta} \qquad \text{for } j = 0, 1, 2, 3, \dots \,. \quad (30)$$

By using the local dispersion relation, Equation (17), this condition on the wavenumber can be rewritten in terms of the wave frequency,

$$\omega^2 = \left[\frac{m^2 \pi^2}{L^2} + \frac{(j + 1/2)^2 \pi^2}{(W - \delta)^2} \right] V_e^2 \,. \quad (31)$$

These frequencies are indicated on Figure 4 using the dashed green curves with $j = 0$ being the lowest curve and $j = 1$ and $j = 2$ appearing at higher frequencies. It is clear from the diagram that a mode of the loop-arcade system can be roughly classified as either a loop mode or an arcade mode, except where the frequencies of the two families of solutions are commensurate. At these points in parameter space, a mode of the system is mixed in character and a classic avoided crossing occurs as the loop width parameter is varied.

The change in behavior as a node slides through the loop boundary is further illustrated in Figure 5, which shows eigenfunctions for a $n = 4$ kink mode (left panels) and a $n = 5$ sausage mode (right panels). The top panels show the magnetic pressure fluctuation and the bottom panels are the axial velocity. Since the axial velocity is purely imaginary when the magnetic pressure fluctuation is purely real, we show the imaginary part of the axial velocity. All eigenfunctions have been normalized to have a peak value of unity.

The three different kink-mode curves correspond to different values of the loop's half-width δ. The three values are printed in the legend, and are also indicated

with the filled squared in the mode diagram, Figure 4. The color of the squares in Figure 4 matches the color of the eigenfunction curves in Figure 5. These three values of the loop width were chosen to fall between avoided crossings in the mode diagram. One can easily determine by inspection that all velocity eigenfunctions for the kink mode have four nodes ($n = 4$), but depending on where the mode falls on the mode diagram in relation to the avoided crossings, there can be zero, two or four nodes within the loop itself. A similar result holds for the sausage mode with five total nodes and a differing number of nodes located within the loop. The three values of the loop width that are illustrated for the sausage mode are indicated with open, colored squares in the mode diagram.

3.2. Are Loop Oscillations Due to a Local Resonance?

The width of a coronal loop compared to its length is typically quite small. This fact has been exploited theoretically, by considering the limit where the width of the loop goes to zero. This so called "thin loop" limit is exceedingly advantageous as it permits the coronal seismologist to ignore any variations across the cross section of the loop. It is not that the loop lacks substructure; the loop may indeed be comprised of a bundle of threads. Instead, the substructure does not matter seismically. The threads oscillate collectively, and for seismic purposes the loop may be treated as a narrow, featureless bundle of field lines (e.g., Terradas et al. 2008).

The equivalent limit for our loop-arcade model is the thin slab limit, where we consider what happens when we let the loop's half-width approach zero, $\delta/L \to 0$. In this limit it is easy to demonstrate that the frequency of the fundamental kink mode, $n = 0$, converges to the well-known result $\omega \to k_z V_e$ (i.e., Edwin & Roberts 1982). That is, the longitudinal phase speed approaches the external Alfvén speed, $\omega/k_z \to V_e$. This can be seen directly in Figure 4, where the gravest mode approaches the arcade's cutoff frequency as $\delta \to 0$. It is also simple to demonstrate that the overtones ($n > 0$) all converge to the eigenfrequencies that the arcade would have in the absence of the loop,

$$\omega^2 \to \left(\frac{n^2 \pi^2}{4 W^2} + \frac{m^2 \pi^2}{L^2} \right) V_e^2 \,. \quad (32)$$

Thus, when the loop is thin, there is a clear separation of the two families of modes: the fundamental mode ($n = 0$) corresponds to a loop mode that resides primarily in the loop and axial overtones ($n > 0$) are arcade modes that reside primarily in the arcade. When the loop is thick (finite δ), the situation becomes more complicated. At low frequency, all of the modes have an energy density confined to the loop. But, at higher frequencies, the modes propagate both inside and outside the loop.

At first blush, this separation of the modes into arcade modes and loop modes for thin loops sounds promising. It suggests that coronal seismology should be able to concentrate on the loop resonance and ignore the detailed properties of the coronal arcade. The initial glee resulting from this impression should be tempered, however. Mode identification turns out to be problematic. Typically, the swaying motion of a coronal loop is relatively easy to observe and measure because the loop

8

is bright. The associated motions within the surrounding arcade may be largely invisible because the arcade is dim and smooth with little spatial variation in brightness. Unfortunately, this means that all kink modes ($n = 0, 2, 4, 6, \ldots$) will look essentially the same, independent of whether they correspond to a loop resonance or an arcade resonance. For all of these modes, the coronal loop will be seen to sway back and forth because all modes lack structure or nodes within the loop itself. Figure 6 illustrates three of the gravest kink modes $n = 0$, 2, and 4 and sausage modes $n = 1$, 3, and 5 in the thin slab limit. The three kink modes are indicated on the mode diagram, Figure 4, with the filled colored circles. The sausage modes are marked with the open circles. The color of the circle corresponds to the color of the eigenfunction curves. It is clear, that within the loop, all of the kink modes have essentially the same eigenfunction and separately so do all the sausage waves. Another view of this is provided in Figure 7, where a snap shot of the oscillating field lines for the same three kink modes are shown. The blue lines correspond to field lines in the arcade and the thick red line shows the position of the loop. Note, the displacement amplitude of each of the illustrated field lines is calculated from the eigenfunctions, Equation (25). As one can see, the shape of the loop looks identical for all three modes.

For the $n = 0$ mode, the wave is a resonance of the loop and the loop is actively participating in the oscillation. For the overtones, $n > 0$, the loop is a bright passive tracer that follows the motion within the surrounding arcade. If you do not directly observe the motions within the arcade, the only observable distinction between the resonance of the loop and resonances of the arcade is the frequency of oscillation. But, the frequency is the quantity that one must measure to seismically assess the properties of the loop.

Most large-amplitude coronal loop oscillations seem to be connected to flares, but the mechanism is not well understood. Often a wave front is seen propagating away from the flare site (Jain et al. 2015; Zhang 2020) and such fronts may be coeval with the initiation of the oscillations. Such a mechanism should indiscrimately excite a broad spectrum of arcade and loop modes. In fact, its hard to imagine how only the loop resonance could be selectively excited while the arcade modes remain dormant. In fact, it seems more likely that the converse would occur: a wavefront launched by a flare impacts the edges of the arcade and preferentially excites the gravest arcade modes, only weakly tickling the loop resonance because the loop is embedded in the arcade.

Misidentification of a mode has unfortunate consequences. How much of an error in a seismic inference is likely? In general the ratio of mode frequencies of an axial overtone to the axial fundamental in the thin loop limit is given by,

$$\frac{\omega_n}{\omega_0} = \left(1 + \frac{n^2 L^2}{4 m^2 W^2}\right)^{1/2} . \qquad (33)$$

Imagine that a flare excites the gravest kink mode of the arcade ($n = 2$), but one mistakenly believes that the oscillation is just of the embedded loop ($n = 0$). For a thin loop, the ratio of the frequencies of the two modes is given by

$$\frac{\omega_2}{\omega_0} = \left(1 + \frac{L^2}{W^2}\right)^{1/2} , \qquad (34)$$

where we have assumed $m = 1$. Note, the frequency ratio only depends on the physical dimensions of the arcade. Since, the seismic estimate of the kink speed is proportional to the wave frequency, the fractional error that is made in the inferred kink speed is equal to the fractional difference between the two mode frequencies. If we assume a loop length of $L = 100$ Mm and an arcade breadth of $2W = 200$ Mm, the resulting fractional error is around a 40% overestimation of the wave speed (and hence the magnetic pressure).

4. DISCUSSION

The goal of coronal seismology is to probe the density and magnetic field strength of a corona loop (and potentially its coronal environment) through the measurement of the resonant oscillation frequencies of the loop. The seismic inferences are therefore highly dependent on the validity of the wave model that predicts the frequencies as functions of the properties of the loop. If a poor model is employed, the seismic deductions will be equally poor. To date, the models used in coronal seismology have been predicated on the axiom that the observed oscillations are resonant kink oscillations of an isolated magnetic loop. In general, the effects of structure in the loop's environment have received only cursory attention. Here we examine two ways in which this axiom can be broken: (1) we question the isolation of coronal loops from other magnetic structures and (2) we explore potential interactions of the loop resonances with the resonances of the magnetic arcade that cradles the loop.

4.1. Coupling with Nearby Structures

Coronal loops are always part of a larger flux system or arcade and these arcades tend to be highly structured. Often many loops can be observed within the same arcade, sometimes visible and sometimes not, as each loop brightens and fades. *In order for the measured frequencies to be a direct diagnostic of the properties of the vacillating loop, the arcade that houses the loop must be weakly structured such that no significant scatterer lies within a skin depth.* Since, the skin depth of a slender magnetic loop is generally quite large, often comparable to the height of the loop itself, the various loops within an arcade are often within a skin depth of each other, as are the edges of the arcade. Thus, the oscillations of most observed loops are the response of a system of coupled loops and the measured frequencies are not just functions of the properties of the loop under observation. Instead, the frequencies depend on the individual properties of all the loops and on the collective properties of the system, such as the separation and spatial organization of the loops (Bogdan & Fox 1991; Luna et al. 2008, 2009; Van Doorsselaere et al. 2008).

4.2. Coupling with Arcade Resonances

MHD fast waves can propagate surprising distances within the corona. Over the typical lifetime of a coronal-loop oscillation, fast magnetic pressure waves can propagate distances that are comparable to the radius of the

Sun. For example, Jain et al. (2015) measure an oscillation lifetime of 5 minutes for several coronal loops excited by a nearby flare. From the wave front launched from the flare site, they estimate a coronal Alfvén speed of 2.5 Mm s^{-1}. Fast waves would therefore travel 750 Mm during the loop oscillation's decay time. Since, the waves can travel along and across field lines, the waves can efficiently propagate everywhere, interacting with all of the flux structures within an active region. Furthermore, the fast waves can travel back and forth many times across a typical active region; thus, any resonances that are present should be excited. It should be no surprise that the entire active region is observed to thrum and quiver after a flare, with each flux system throbbing coherently.

If the resulting modes of the arcade possess a frequency that is similar to a frequency of the modes of a coronal loop that is embedded in the arcade, the loop oscillations and the arcade oscillations will be coupled. In our simple model, such coincident frequencies only occur for the lateral overtones of the loop and all such modes are of mixed character. The fundamental kink mode maintains it's purity as a loop oscillation; although we note that in the thin loop limit, the wave's skin depth in the arcade becomes infinite because the wave's longitudinal phase speed approaches the Alfvén speed of the arcade. This behavior is a consequence of the slab geometry (e.g., Edwin & Roberts 1982) and does not occur in cylindrical geometry where the kink speed is intermediate between the Alfvén speeds of the loop and the environment.

4.3. *Mode Misidentification*

Arcade resonances can masquerade as a loop resonance. Once again, we emphasize that without being able to observe the eigenfunction within the surrounding arcade and along the loop at multiple positions, one can never be sure which modes have been excited and which modes are being measured. For many events, such additional information may not be forthcoming. However, in some cases, oscillations can be observed within the surrounding arcade. For example, Allian et al. (2019) used an autocorrelation technique to identify the correlated oscillation of a background of dim loops within the surrounding aracade. While they did not measure the axial eigenfunction of arcade oscillations, they did demonstrate that the arcade as a whole oscillated at nearly the same frequency as the loop. With further refinement, it might be possible to use similar correlation techniques to identify the presence or absence of nodes within the arcade by seeking for phase differences between different parts of the arcade. Another possibility is to examine several loops within the same arcade. If the loops are well separated (further than a skin depth), yet oscillate with the same phase, we may be observing a low-order arcade mode. Similarly, if the two loops oscillate with anti-phase it is likely that the arcade oscillation has a node in between the two loops.

A variety of previous efforts have detected multiple conincident frequencies of oscillation for a single coronal loop (Verwichte et al. 2004; Van Doorsselaere et al. 2007; De Moortel & Brady 2007; Li et al. 2017; Duckenfield et al. 2018). Previously, such detections have been implicitly assumed to be the consequence of the coexistence of modes corresponding to different **longitudinal** orders or overtones. Typically, two frequencies have been detected, and the lowest frequency is assumed to be that of the fundamental longitudinal mode ($m = 1$) and the higher frequency concomitant with the first longitudinal overtone ($m = 2$). The ratio of frequencies of such longitudinal overtones has been proposed as a diagnostic for variations along the loop in the mass density, magnetic field strength, and loop radius (Andries et al. 2005; Goossens et al. 2006; Dymova & Ruderman 2006; Díaz et al. 2007; McEwan et al. 2008; Ruderman et al. 2008; Verth & Erdélyi 2008; Orza et al. 2012; Jain & Hindman 2012). In observations, it is rare for a majority of the length of the loop to be clearly visible, and hence it is rare that one can verify which longitudinal modes have been excited by seeking the presence of nodes. Thus, it is often impossible to know if the two frequencies actually correspond to different longitudinal orders (different m). Our work here suggests another possibility; the higher frequency oscillation could correspond to an **axial** overtone of the host arcade ($n > 0$) instead of a longitudinal overtone ($m > 1$). Of course, both mechanisms could be, and probably are, at work simultaneously. Since, Equation (33) suggests that the effects of axial overtones can be assessed through the aspect ratio of the arcade W/L, we strongly urge that observations of an oscillation event attempt to characterize not only the length of the loop, but the width of the host arcade.

4.4. *Conclusions*

Coronal seismology has long sought to model coronal loop oscillations as trapped waves in a 1D waveguide that is isolated from other coronal structures. Typically the selection of oscillation events is accomplished by looking for loops with high brightness contrast that undergo large-amplitude motions that are easy to detect and measure. Other than an obvious and justifiable bias towards loops that lack overlapping and obscuring foreground and background features, the magnetic environment of the loop is usually not a selection criterion. Here we have explored a few ways in which the environment of the loop can break the basic assumptions implicit to coronal seismology. In particular, we have shown that the lateral evanescent length, or the skin depth, of kink oscillations can be remarkably long in the fluid surrounding the loop. This means that one must be extremely judicious when selecting candidate events for seismic analysis. The corona around the loop should be nearly featureless.

We have also explored how modes of the loop can couple to modes of the surrounding arcade. When this happens, the waveguide takes on a multi-dimensional geometry. Our model is 2D, but it is easy to imagine that the true waveguide could be fully 3D (e.g., Hindman & Jain 2015; Thackray & Jain 2017; Hindman & Jain 2018). We also demonstrate that observations made of the motion at a single position along the loop is insufficient to allow unique identification of the mode of oscillation. Proper identification of the mode is essential to correctly deduce the kink speed and other properties of the loop. Once, again our results suggest that event selection needs to take the environment of the loop into consideration. Any arcade resonances need to have sufficiently disparate frequencies that coupling is weak.

Finally, in a broader context, coronal seismology needs more thorough testing. Currently, we lack a basic un-

derstanding of the reliability and accuracy of seismic interferences. The community needs to apply seismic techniques to a large sampling of loops for which magnetic field strength and geometry estimates are available through spectroscopic and stereoscopic observations.

REFERENCES

Allian, F., Jain, R., & Hindman, B.W. 2019, ApJ, 880, 3

Andries, J., Goossens, M., Hollweg, J.V., Arregui, I., & Van Doorsselaere, T. 2005, A&A, 430, 1109

Anfinogentov, A., Nisticò, G., & Nakariakov, V.M. 2013, A&A, 560, 107

Arregui, I., Terradas, J., Oliver, R., & Ballester, J.L., 2007, Sol. Phys., 246, 213

Aschwanden, M.J., Fletcher, L., Schrijver, C.J., & Alexander, D. 1999, ApJ, 520, 880

Bogdan, T.J. & Fox, D.C. 1991, ApJ, 379, 758

De Moortel, I. & Brady, C.S. 2007, ApJ, 664, 1210

Díaz, A.J., Donelly, G.R., & Roberts, B. 2007, A&A, 476, 359

Díaz, A.J., Oliver, R., & Ballester, J.L. 2003, A&A, 402, 781

Duckenfield, T., Anfinogentov, S. A., Pascoe, D. J., & Narkariakov, V. M. 2018, ApJ, 854, L5

Dymova, M.V. & Ruderman, M.S. 2006, A&A, 459, 241

Edwin, P.M. & Roberts, B. 1982, Sol. Phys., 76, 239

Edwin, P.M. & Roberts, B. 1983, Sol. Phys., 88, 179

Goddard, C.R., Nisticò, G., Nakariakov, V.M., & Zimovets, I.V. 2016, A&A, 585, A137

Gruszecki, M., Murawski, K., Solanki, S.K., & Ofman, L. 2007, A&A, 469, 1117

Goossens, M., Andries, J., & Arregui, I., 2006, RSPTA, 364, 433

Hindman, B.W. & Jain, R. 2015, ApJ, 814, 105

Hindman, B.W. & Jain, R. 2018, ApJ, 858, 6

Jain, R. & Hindman, B.W. 2012, A&A, 545, 138

Jain, R., Maurya, R.A., & Hindman, B.W. 2015, ApJ, 804, L19

Joarder, P.S. & Roberts, B. 1992, A&A, 256, 264

Lemen, J.R., Title, A.M., Akin, D.J., et al. 2012, Sol. Phys., 275, 17

Lenz, D.D., DeLuca, E.E., Golub, L., Rosner, R. & Bookbinder, J.A., 1999, ApJ, 517, L155

Li, H., Liu, Y., & Tam, K.V. 2017, ApJ, 842, 99

Luna, M., Terradas, J., Oliver, R., & Ballester, J.L. 2008, ApJ, 676, 717

Luna, M., Terradas, J., Oliver, R., & Ballester, J.L. 2009, ApJ, 692, 1582

McEwan, M. P., Díaz, A.J., & Roberts, B. 2008, A&A, 481, 819

Nakariakov, V.M. & Kolotkov, D.Y. 2020, ARA&A, 58, 441

Nakariakov, V., Ofman, L., DeLuca, E., Roberts, B., & Davila, J.M. 1999, Sci, 85, 862

Nechaeva, A., Zimovets, I.V., Nakariakov, V.M., & Goddard, C.R. 2019, ApJS, 241, 31

Nisticò, G., Nakariakov, V.M., & Verwichte, E. 2013, A&A, 552, 57

Orza, B., Ballai, I., Jain, R., & Murawski, K. 2012, A&A, 537, A41

Pascoe, D.J. & De Moortel, I. 2014, ApJ, 784, 101

Reale, F. 2014, LRSP, 11, 4

Roberts, B., Edwin, P.M., & Benz, A.O. 1984, ApJ, 279, 857

Roberts, B. 2019, MHD Waves in the Solar Atmosphere (Cambridge, UK: Cambridge University Press)

Ruderman, M.S. 2009, A&A, 506, 885

Ruderman, M.S., Verth, G., & Erdéyi, R. 2008, ApJ, 686, 694

Schrijver, C.J. & Brown, D.S. 2000, ApJ, 537, L69

Schrijver, C.J., Aschwanden, M.J., & Title, A.M. 2002, Sol. Phys., 206, 69

Terradas, J., Oliver, R., & Ballester, J.L. 2006, ApJ, 650, L91

Terradas, J., Arregui, I., Oliver, R., Ballester, J.L., Andries, J., & Goossens, M. 2008, ApJ, 679, 1611

Thackray, H. & Jain, R. (2017), A&A, 608. 108

Van Doorsselaere, T., Nakariakov, V.M. & Verwichte, E. 2007, A&A, 473, 959

Van Doorsselaere, T., Ruderman, M.S., & Robertson, D. 2008, A&A, 485, 849

Van Doorsselaere, T., Verwichte, E., & Terradas, J. 2009, Space Sci. Rev., 149, 299

Verth, G. & Erdélyi, R. 2008, A&A, 486, 1015

Verwichte, E., Nakariakov, V.M., Ofman, L., & Deluca, E.E. 2004, Sol. Phys., 223, 77

Verwichte, E., Aschwanden, M.J., Van Doorsselaere, T., Foullon, C., & Nakariakov, V.M. 2009, ApJ, 698, 397

Wang, T., Ofman, L., Davila, J.M., & Su, Y. 2012, ApJ, 751, L27

Wills-Davey, M.J. & Thompson, B.J. 1999, Sol. Phys., 190, 467

Winebarger, A.R., Warren, H.P., & Mariska, J.T. 2003, ApJ, 587, 439

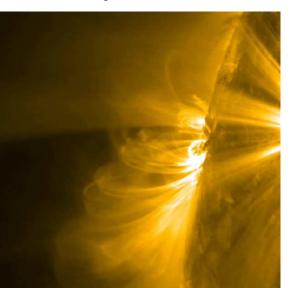Zhang, Q.M. 2020, A&A, 642, 159

FIG. 1.— A still image that presents the first frame of a movie sequence that is provided as a separate ancillary file (figure1.mp4). The still and the animation show an arcade of magnetic field lines in the corona located on the solar limb. The sequence of images was obtained by AIA in the Fe IX 171 Å bandpass. Just after the animation begins, a flare occurs causing the arcade to spasm. The animation clearly demonstrates that the entire arcade and the larger active region participate in the oscillation and that MHD fast waves propagate across magnetic field lines.
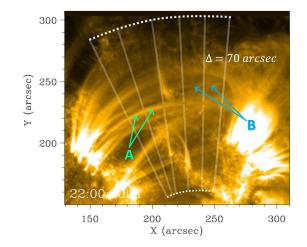

FIG. 2.— Snapshot of NOAA AR 1283 taken on 2011 September 6 by AIA in the 171 Å passband. There are a multitude of coronal loops evident, many embedded in a common magnetic arcade. The two loops studied by Jain et al. (2015) are indicated and labeled A and B. Since each of these loops has a length of 160 Mm, the lower limit for the skin depth of each is 50 Mm or 70 arcsec. Using the partially transparent yellow lines, we have indicated a distance of 70 arcsec on the plane of the sky to either side of loop A. The region between the dotted white lines indicates the approximate region that lies within a single skin depth of loop A. Loops A and B are clearly well within each others near field and hence, are strongly coupled. In fact, most of field of view, and correspondingly much of the active region, should be coupled to the oscillating loops.
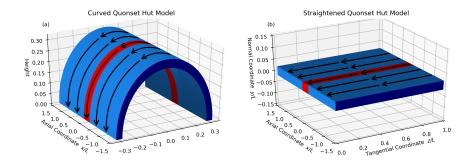
Fig. 3.— Geometry of our model of a coronal loop embedded in a coronal arcade. (a) The arcade is a thin, curved sheet of plasma. The axis of the arcade $\hat{\boldsymbol{x}}$, the magnetic field lines, and the curvature vector are all mutually orthogonal. In the figure the arcade is indicated by the blue sheet and the magnetic field lines by the black curves. Each field line intersects the photosphere twice. The loop is a segment of the arcade (shown in red), that lies in the center. (b) We ignore the curvature of the arcade and loop, and work in slab geometry. The coordinate that is parallel to the magetic field is z. The coordinate parallel to the axis of the arcade is x, and the coordinate normal to the sheet is y.
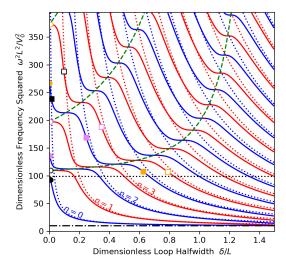

Fig. 4.— Mode diagram that indicates the frequency of modes as a function of the loop's half width. The blue curves correspond to kink modes and the red curves to sausage modes. All modes correspond to the longitudinal fundamental, $m = 1$. The solid curves indicate the modes of the loop-arcade system and the dotted curves show the resonances of the loop in isolation, in the limit of large loop overdensity ($f \gg 1$) and extremely wide arcade ($W \gg \delta$). The axial order, n, of each modal curve is indicated for the first four overtones. The dotted horizontal line indicates the cutoff frequency for the arcade, $m\pi L/V_e$, and the dot-dashed line indicates the cutoff for the loop, $m\pi L/V_0$. Waves with frequencies above the cutoff are laterally propagating within the associated region. The dashed green curves indicate the modes of the arcade and correspond to where a node in the axial velocity is coincident with the boundary between the arcade and loop. For each dispersion curve, as the width of the loop decreases, the frequency increases. Whenever a node moves from inside the loop to outside (and the dispersion relation crosses a green dashed curve), an avoided crossing occurs. These crossings can be thought of as the parameter values for which a mode of the arcade has the same frequency as a mode of the loop. The colored squares and circles indicate modes that have eigenfunctions that are illustrated in subsequent figures. The filled squares are kink modes with four total axial nodes in the velocity eigenfunction. The open squares are sausage modes with five nodes. The eigenfunctions are illustrated in Figure 5. The circles correspond to kink modes (filled) and sausage modes (open) in the thin-loop limit, and their eigenfunctions are shown in Figure 6.
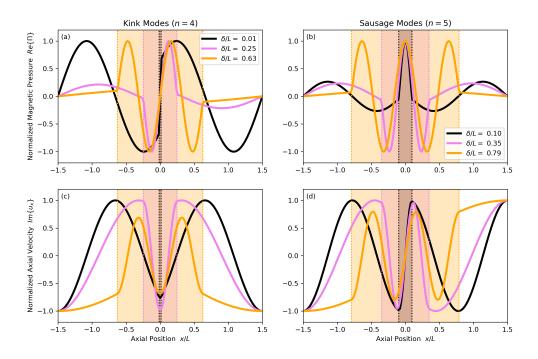
FIG. 5.— Eigenfunctions for a selection of kink modes (left panels) and sausage modes (right panels). The upper panels show the magnetic pressure fluctuation and the bottom panels present the axial velocity. All of the kink modes lie on the $n = 4$ dispersion curve in Figure 4 and are indicated by the filled squares in that figure. Accordingly all of these kink modes have four nodes in their eigenfunctions for the axial velocity. Similarly, all of the sausage modes have five nodes, lie on the $n = 5$ dispersion curve, and are indicated by the open squares. The color of each curve indicates which mode is being plotted, with the same color used to label the mode in Figure 4. Since, the modes are for different values of the loop's half-width, δ, the region occupied by the loop is indicated by the color of the shaded regions. The yellow color indicates the widest loop, and taupe the narrowest.
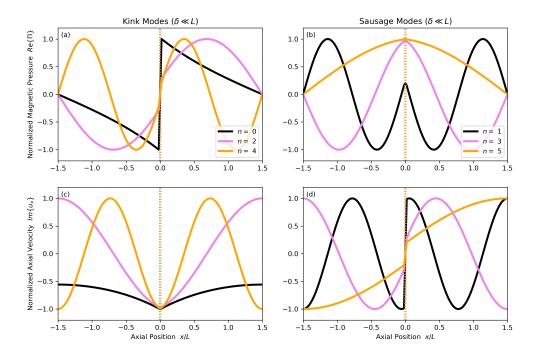
FIG. 6.— Eigenfunctions for a selection of kink modes (left panels) and sausage modes (right panels) that are within the thin loop limit. The upper panels show the magnetic pressure fluctuation and the bottom panels present the axial velocity. The three kink modes correspond to three different axial orders, $n = 0$, 2, and 4. The three modes that are illustrated are indicated on the mode diagram, Figure 4, with filled circles. The color of the circle corresponds to the color of the eigenfunction curve. Similarly, the three sausage modes are for the first three odd orders, $n = 1$, 3, and 5. They are indicated in the mode diagram by the open circles. The $n = 0$ is the only mode that is laterally evanescent within the arcade and as such is a loop resonance. All of the other modes propagate within the arcade and are arcade resonances.
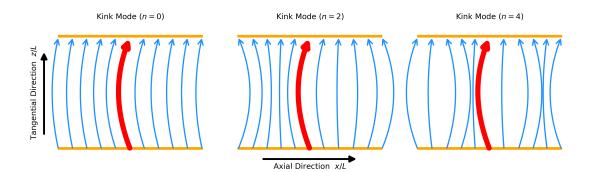

FIG. 7.— Snapshot of the displacement of field lines caused by three different kink modes, $n = 0$, 2, and 4. The gold lines indicate the foot points where the field lines in the arcade intersect the photosphere. The red curved red arrow shows the position of the coronal loop. Note, the displacement of the loop is same for all three modes. The blue arrows indicate the displacement of field lines outside the loop within the arcade. All differences between the three modes occur within the arcade. Often the motions within the host arcade are invisible due to dimness and poor spatial contrast. Thus, all three of these modes would look the same if all one can see is the coronal loop. This can lead to mode misidentification and substantial error in the seismic measurement of loop properties.